Three-Dimensional Flexible Thermal Sensor for Intravascular Flow Monitoring

Rui Tang, Hai Huang, Yong Mo Yang, Jonathon Oiler, Mengbing Liang, and Hongyu Yu, *Member, IEEE*

***Abstract*— A novel design and assembly technology is developed for a three-dimensional (3-D) flexible thermal flow sensor based on convective heat transfer to reduce detection error caused by position variation of a sensor inside the flow of narrow and curved geometries, such as coronary artery. The 3-D sensor has three independent sensing elements equally distributed around the catheter tube. This arrangement introduces three independent information channels, and cross-comparisons are used to provide accurate flow measurement. The resistance of the sensing elements is measured at ∼1–1.2 kΩ with the temperature coefficient of resistance at 0.086%/°C. Using a constant-current circuit, the three sensing elements are heated to ∼10 °C above ambient temperature. Flow testing is implemented in a pipe channel at two positions: on the wall and along the center line. Experimental results from these two positions are discussed and computational fluid dynamic simulation based on Newtonian fluid properties is implemented, showing comparable results within an acceptable range of experimental to simulation errors. Therefore, we demonstrate the capability of 3-D thermal flow sensor for detecting the position of the catheter in the flow channel, thereby providing an accurate flow measurement.**

***Index Terms*— Micro-electro-mechanical systems (MEMS) thermal sensors, polymer, 3-D packaging, shear stress.**

I. Introduction

ATHEROSCLEROSIS, a disease that primarily affects the outer edges of blood vessel bifurcations, is the leading cause of death in the industrialized world. Blood flows differently at bifurcations, where the vessel splits from one channel into two channels, compared to the more straight regions of an artery [1]. Along the medial wall (inner wall associated with the bifurcation), wall shear stress (the tangential frictional force along the arterial wall) is high. Along the lateral wall (outer wall associated with the bifurcation), the flow is slow and oscillatory along the lateral wall. This flow pattern results in a significantly lower amount of wall shear stress [2]. This zone of low shear stress along the lateral arterial wall can allow for the accumulation of plaque, forming atherosclerotic lesions which can rupture and induce clotting of the vessel at the point of rupture or farther downstream. The build-up of these plaques cause tell-tale changes in the local flow field low shear stress upstream of the lesion, high shear stress at the throat of the lesion, and oscillatory flow downstream [3] where more plaque can accumulate. Therefore, development of atherosclerosis can be identified and studied by measurement of the flow properties, especially wall shear stress field.

Micro-Electro-Mechanical Systems (MEMS) sensors have been developed to measure wall shear stress. One of the most common methods involves hot film thermal anemometry [4]–[6]. To relate heat transfer to flow properties in the complicated arterial geometry, one-dimensional (1-D) polymer-based thermal flow sensors were previously introduced into the arterial system with *in-vivo* experiments on New Zealand Rabbits. The flow sensors' primary advantages were structural flexibility, biocompatibility and small size [7]. However, this 1-D sensor suffered from limited data collection ability and large experimental errors. Since the blood velocity varies with the radial position, the sensor output was affected by variations in catheter position and sensors orientation inside the artery. One possible solution is to rotate the 1-D sensor to ensure that the sensing element is facing the blood flow rather than the wall or make the sensor steerable [7]–[10]. However, it is very difficult to monitor and manipulate the sensor intravascularly.

Another recent work was implementing thermal flow sensor in medical guide wires of 360 μm in diameter [17], [18]. Due to its smaller size, the sensor potentially allows for an easier, more accurate and reliable CAD diagnosis [19]. However, with the decreasing of the invasive instrument size, the fabrication and packaging becomes more and more challenging, complicated and costly. Only 1-D pressure and/or flow sensing functionalities were successfully integrated in this type of small guide wires. It was not optimized for flow measurement since it had the same issues with 1-D catheter based sensor.

The 3-D thermal flow sensor reported here improves upon previous work by having three independent sensing elements symmetrically distributed around the wall of catheter tube, which forms a plane perpendicular to the flow direction. With this novel structure, at least one sensing element is ensured to face the flow field away from the artery wall which will provide a more accurate reading, no matter how the sensor is positioned. Meanwhile, by comparing the different readings of all elements, the position of the sensor within the flow channel can be inferred. By being able to detect the position of the catheter within the flow channel, the 3-D thermal flow sensor

Manuscript received March 11, 2013; accepted May 3, 2013. Date of publication May 29, 2013; date of current version September 4, 2013. This work was supported in part by the U.S. National Science Foundation CMMI-0928502. The associate editor coordinating the review of this paper and approving it for publication was Dr. Ravinder S. Dahiya.

R. Tang, H. Huang, and M. Liang are with the School of Electrical, Computer and Energy Engineering, Arizona State University, Tempe, AZ 85287 USA (e-mail: rtang4@asu.edu; Hai.Huang.3@asu.edu; mliang8@asu.edu).

Y. M. Yang was with the School of Electrical, Computer and Energy Engineering, Arizona State University, Tempe, AZ 85287 USA. He is now with Intel, Chandler, AZ 85248 USA (e-mail: Yongmo.Yang@asu.edu).

J. Oiler is with the School of Earth and Space Exploration, Arizona State University, Tempe, AZ 85287 USA (e-mail: Jonathon.Oiler@asu.edu).

H. Yu is with the School of Electrical, Computer and Energy Engineering and the School of Earth and Space Exploration, Arizona State University, Tempe, AZ 85287 USA (e-mail: hongyu.yu@asu.edu).

Color versions of one or more of the figures in this paper are available online at http://ieeexplore.ieee.org.

Digital Object Identifier 10.1109/JSEN.2013.2264623

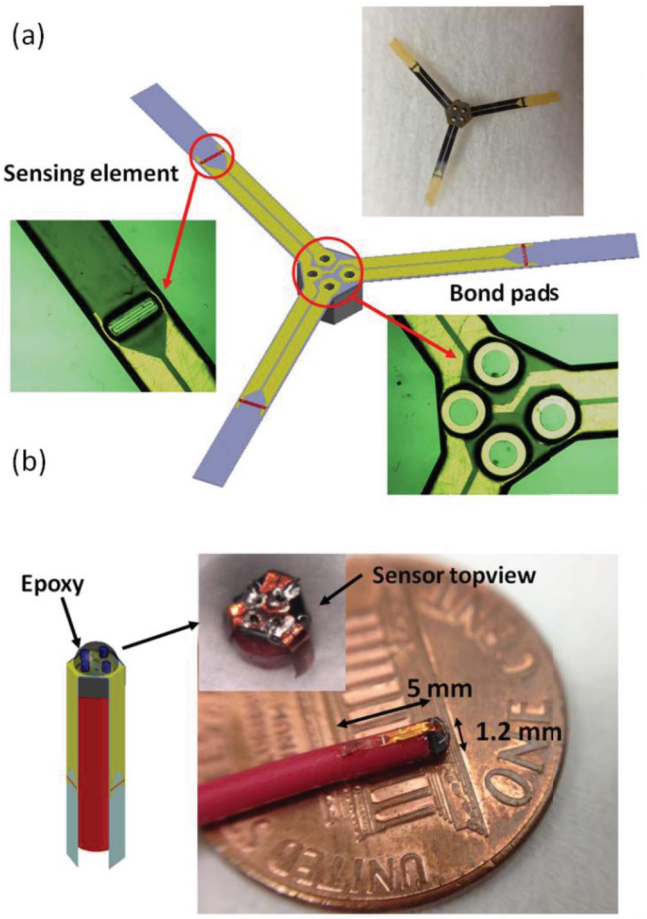

Fig. 1. (a) Unwired sensing device. (b) Sensing device assembled with external wires.

can realize more accurate assessment of intravascular heat transfer and flow properties with the help of computational fluid dynamics (CFD) simulation.

II. Sensor Design and Assembly

A. Sensor Design

As discussed in introduction, the 3-D thermal flow sensor is designed with three sensing elements separated by 120° spacing around the catheter tube. Although more sensing elements could be integrated, it would require larger catheter size and increase cost, since more bond pads for external connection will be employed.

The 3-D thermal flow sensor was similarly to a small cylinder (1.2 mm in diameter) consisted of sensing device and external wires (Fig. 1). In order to make this type of structure, novel fabrication of sensing device and packaging method were developed. The unwired sensing device was designed as a "fan" shape with a silicon substrate cube in the center with thickness of 500 μm and three "blades" of Parylene-C encapsulated sensing elements (Fig. 1(a)). The sensing element and bond pads were sandwiched by Parylene-C layers which provide electrical insulation and mechanical support. Each Parylene-C blade was 5 mm in length, 580 μm in width, and approximately 21 μm in thickness.

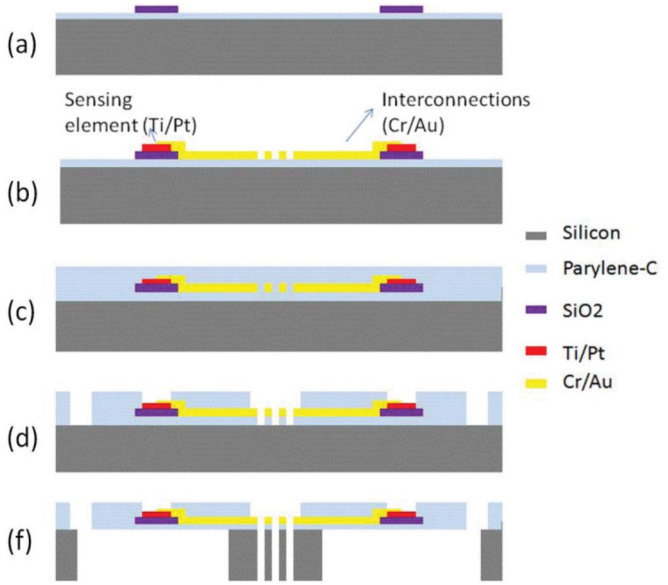

Fig. 2. Fabrication of the sensor: (a) deposition of Parylene-C and silicon dioxide; (b) deposition and patterning of sensing elements and interconnections; (c) deposition of another layer of Parylene-C; (d) pattering Parylene-C; and (e) backside DRIE etching and sensor releasing.

B. Fabrication

The sensing element was fabricated using surface micromachining with biocompatible materials including Titanium (Ti) and Platinum (Pt). The fabrication process of sensing device is as follows: 1) start with a bare silicon wafer, deposit a thin (10 μm) Parylene-C layer (with A-174 adhesion promoter) on silicon wafer; 2) deposit and pattern a 0.1 μm silicon dioxide to form an etching stop to prevent Reactive-Ion Etching (RIE) through Parylene-C in a later step (20 nm Chromium (Cr) was used to enhance the adhesion between silicon dioxide and Parylene-C); 3) deposit Ti/Pt layers with thickness of 0.12 μm/0.02 μm and lift-off these layers to form a 10 μm wide metal strips as the resistive sensing element, and after that, deposit and pattern Cr/Au 0.02 μm /0.6 μm for interconnection between sensing element and bond pads; 4) deposit and pattern second 10 μm Parylene-C layer to provide structural support and electrical insulation. Because the etch rate between Parylene-C and photoresist is similar, more than 20 μm thick photoresist is needed accordingly; 5) perform backside photolithography of silicon wafer, then hard bake for 30 minutes; 6) use Deep Reactive-Ion Etching (DRIE) to etch silicon from backside to release the sensor structure leading to the final sensing device, shown in Fig. 2.

C. Packaging

After the sensing device was released, four electrical coaxial wires (Precision Interconnect, Portland, OR) were inserted through backside holes to the topside Cr/Au bond pads (three for the sensing elements and one for common ground). Silver epoxy (H20E, Epoxy Technology, Inc.) was then used to connect the external wires and bond pads under microscope. The silver epoxy was fully cured at 60 °C over 6 hours. A small wire sheath was used to wrap these small external wires and provide support to Parylene-C wings. After being

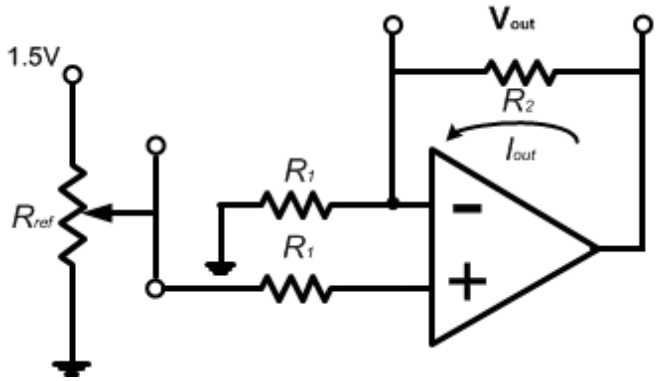

Fig. 3. Schematic of constant-current mode driving circuit. R_2 represents the sensor resistor.

connected with external wires through the center cube, these blades were bent and mounted to nonadjacent side surfaces of silicon substrate cube and wire sheath. Finally, biocompatible epoxy (EPO-TEK 301: Epoxy Technology, Billerica, MA, USA) was applied to cover bonds on the silicon substrate cube and provide electrical insulation (Fig. 1(b)).

III. Experiment

A. Sensor Calibration

The temperature coefficient of resistance of the sensing elements was measured on a precision temperature control hotplate. Then, the 3-D thermal flow sensor was connected to a constant-current (CC) circuit providing 1.05 mA current through each sensing element, Fig. 3) and each sensing element was heated up about 10 °C above ambient temperature (23.4 °C).

For this thermal flow sensor, the output signal is the voltage change across the sensing element. In order to measure flow properties, specifically shear stress, a relation between shear stress and output voltage needs to be developed through calibration. Based on the heat transfer principle, the output voltage of the thermal flow sensors was sensitive to the fluctuation in ambient temperature. The temperature overheat ratio (α_T) is defined as temperature variations of the sensor over the ambient temperature (T_0) [15], [16]:

$$\alpha_T = \frac{(T - T_0)}{T_0} \tag{1}$$

where T denotes the temperature of the sensor. The relation between resistance and temperature overheat ratios is expressed as

$$\alpha_R = \frac{(R - R_0)}{R_0} = \alpha_T T_0 \alpha = \alpha (T - T_0) \tag{2}$$

where α is the TCR. For shear stress measurements, typically a high overheat ratio (~2.8 %) is used by passing higher current and by generating a "hot" sensing element to stabilize the sensor.

A 2-D PDMS channel with a small trench was built (Fig. 4(a)) to calibrate the 3-D thermal flow sensor. The small trench allows the 3-D sensor to be rotated inside the channel, allowing all three sensing elements to be individually calibrated. A syringe pumps system (Harvard Apparatus PHD2000) was used to provide water flows at several flow rates (range from 10 mL/min to 100 mL/min). We can directly obtain the relationship between the output voltage change and flow rate through this calibration system. For a Newtonian fluid at steady state, the theoretical shear stress value in relation to the flow rate in the 2-D flow channel was established using the formula based on the analysis of Truskey *et al* [14]:

$$\tau_{xy}\big|_{y=H/2,x=0} = \frac{\mu Q}{W H^2 - \sum_{n=0}^{\infty} \frac{96 H^3}{(2n+1)^5 \pi^5 \cosh\left(\frac{(2n+1)\pi W}{2H}\right)} \exp\left(\frac{(2n+1)\pi W}{2H}\right)} \left(6 - \sum_{n=0}^{\infty} \frac{48}{(2n+1)^2 \pi^2 \cosh\left(\frac{(2n+1)\pi W}{2H}\right)}\right)$$
$$y \in (-H/2, H/2), x \in (-W/2, W/2) \tag{3}$$

where τ is the wall shear stress, μ is the blood viscosity, and H and W are the height and the width of the flow channel, respectively ($H/W = 0.222$).

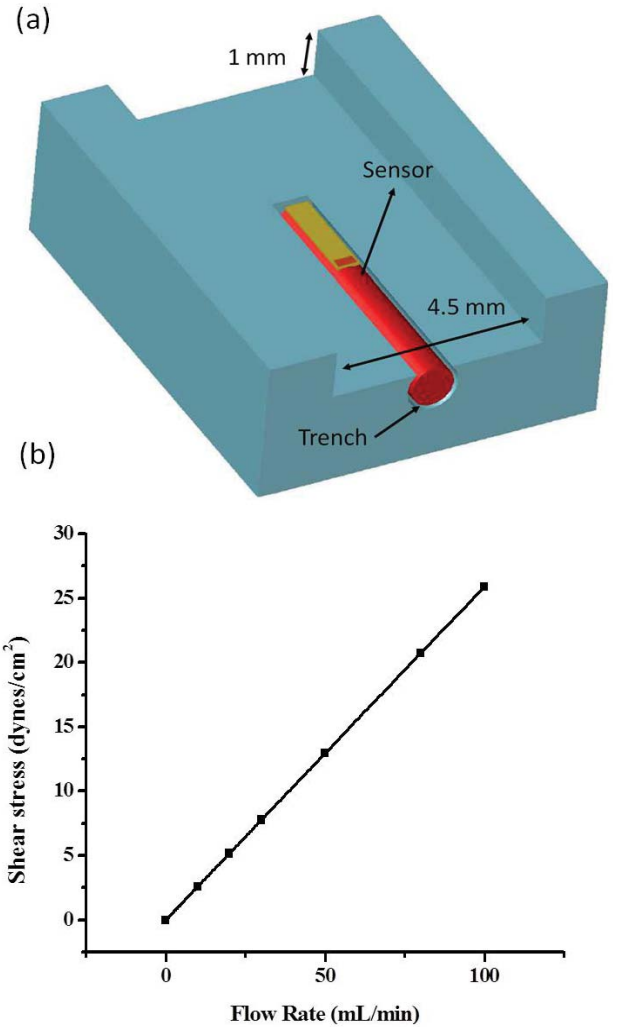

Fig. 4. (a) Schematic diagram of 2-D PDMS channel for sensor calibration. The sensor body was inserted into the trench underneath the channel at a sufficient entrance length to allow for fully developed laminar flow before reaching the sensor. (b) The relation between flow rate and wall shear stress was obtained.

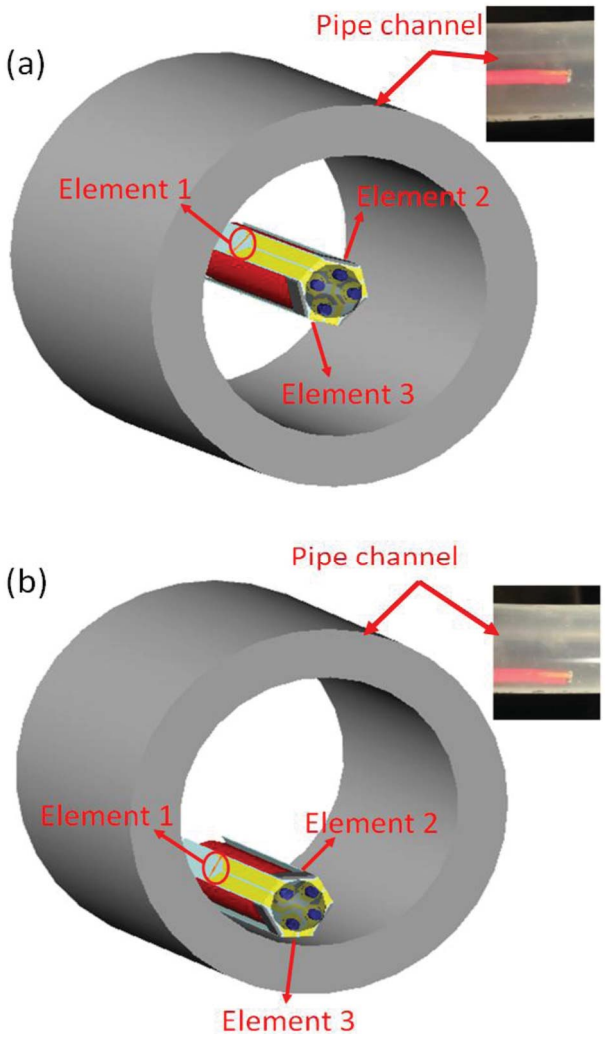

Fig. 5. The sensor was inserted into the channel and fixed in two positions: (a) sensor was placed in the center of the channel and (b) sensor was attached to the wall of the channel.

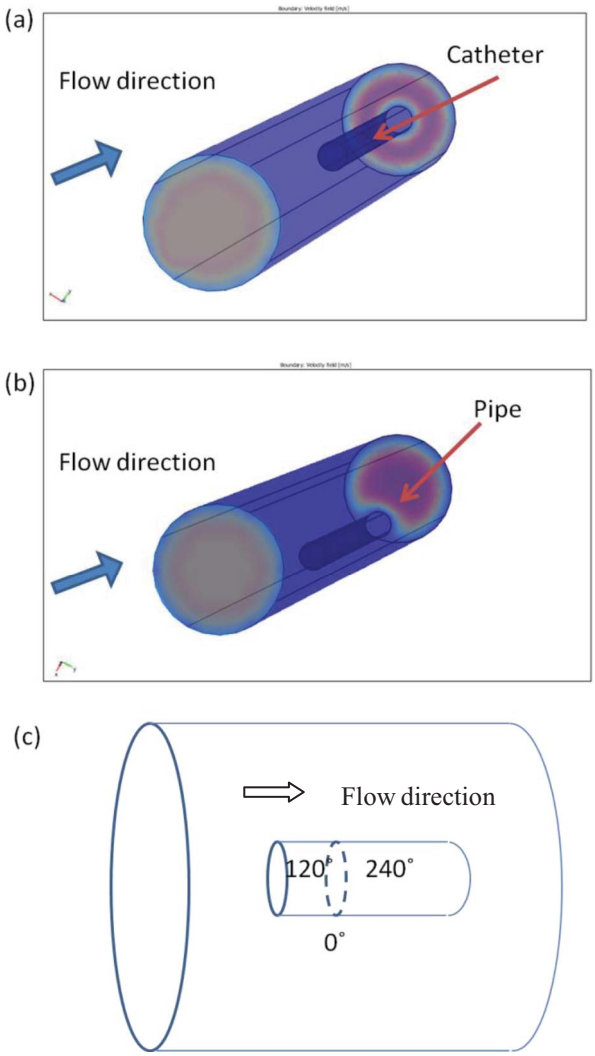

Fig. 6. CFD simulations of different positions. (a) The sensor is in the center line of the pipe. (b) The sensor is on the wall of the pipe. (c) The distribution of sensing elements.

The formula was implemented in Matlab to calculate wall shear stress under different flow rates in the calibration channel.

B. Flow Test

The thermal flow sensor has three independent sensing elements symmetrically distributed on its wall (Fig. 1). These sensing elements form a plane perpendicular to the flow direction, thus, the sensor can detect its location in the flow channel by the difference among all element readings.

In order to prove this concept, the 3-D thermal flow sensor was tested in a pipe channel (5 mm in diameter) with different flow rates controlled by a pump system. The diameter ratio (pipe diameter/sensor diameter) of 4.5 would minimize the pressure and shear stress disturbance caused by insertion of the sensor [10]. Meanwhile, the Intravascular Shear Stress (ISS) elevation factor (ratio of actual shear stress on the sensor/wall shear stress in the absence of catheter) will increase as the diameter ratio of pipe diameter/sensor increases. Based on this consideration, a value near 4.5 (about 4.2) was chosen for our flow test to reduce the insertion effect of the sensor. The ISS elevation factor through our simulation is 2.53 which agrees the value 3 in the reference [10]. The length of pipe channel is set to be more than 10 times of diameter to provide sufficient entrance length for the flow to fully develop. The three sensing elements were labeled as element 1, element 2 and element 3.

Next, the sensor was inserted into the channel and fixed in two positions: (a) sensor was attached to the wall of the channel; (b) sensor was placed at the center of the channel. For position (a), element 3 was placed against the wall of channel (although there was a very small separation between element 3 and the wall, we defined this position as "attached"). Element 1 and element 2 were facing the flow field (Fig. 5(a)). For position (b), the sensor was placed in the center of the channel and all three sensing elements were facing the flow field (Fig. 5(b)).

C. CFD Simulation

Computational fluid dynamic (CFD) simulation was implemented for Newtonian fluid to simulate shear stress in a

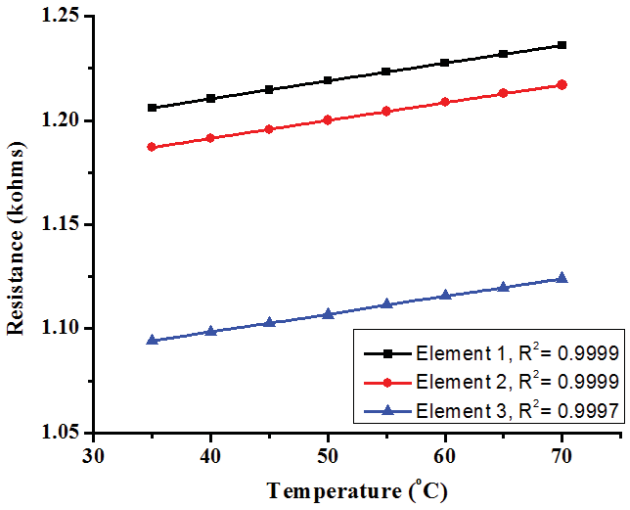

Fig. 7. Plot of sensing element (Ti/Pt) resistance versus temperature. A linear relation was established over the temperature ranging from 25 °C to 70 °C. The TCR was approximately 0.086 %/°C.

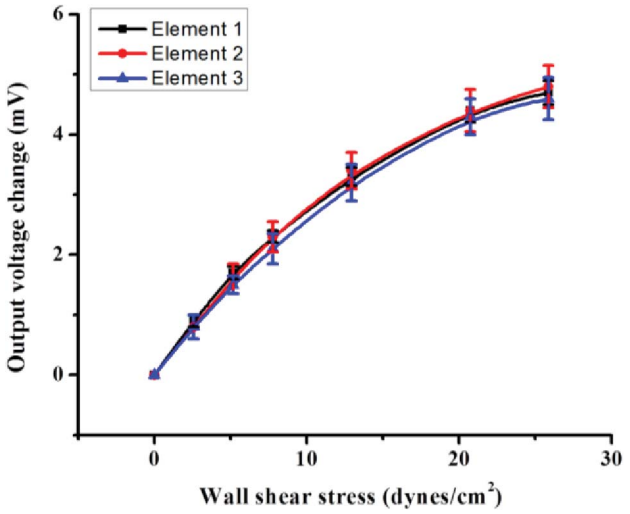

Fig. 8. Calibration curve for sensor output voltage change and wall shear stress in response to water flow. Output voltage was plotted as a function of wall shear stress in the PDMS channel.

pipe channel in order to compare with the experimental measurements (Fig. 6). The pipe channel with catheter model was constructed and meshed using COMSOL Multiphysics software. The grid was generated by meshing the inlet surface using map mesh to create structured mesh, followed by generating a volume mesh by sweeping the mesh node patterns that specified the inlet surface as the "source" faces. For simulation of wall shear stress, boundary layers immediately adjacent to the wall were constructed to generate sufficient information for characterization of the large fluid velocity gradients near the wall. The diameter of the pipe was set at 5 mm and the catheter was 1.2 mm. The total channel length was set at 10 times of the diameter to provide sufficient entrance length for the flow to develop [12]. The water flow was simulated by applying the 3-D Navier–Stokes equations. The governing equations, including mass and momentum equations, were solved for laminar, incompressible, and Newtonian flow. The wall of the pipe was assumed to be rigid and impermeable. No-slip boundary condition was implemented along the inner walls. The flow field was initialized by propagating the constant time-averaged inlet velocity profile downstream into the computational domain. The initial pressure was set to zero in the entire domain.

IV. Experimental Results and Discussion

The resistance of the sensing elements was measured at approximately 1-1.2 kΩ with the temperature coefficient of resistance (TCR) at approximately 0.086 %/°C (Fig. 7). The relation between the resistance and temperature was linear, suggesting that the TCR over this temperature range remained constant.

The calibration curve between the output voltage change and shear stress was generated, shown in Fig. 8. In lower shear stress region (0-12 dynes/cm^2), output voltage change increased linearly as flow shear stress increased. The use of Ti and Pt as the sensing element materials provides a maximum sensitivity of 0.25 mV/(dynes/cm^2). Then, the curve gradually tended to saturate in higher shear stress region with the slope becoming flatter (at higher than 15 dynes/cm^2).

The reason can be found from qualitative analysis on the sensor's operating principle which is based on convective cooling of a heated sensing element as fluid flows over its surface. The heat transfer from the heated surface to the fluid depends on the flow characteristics in the viscous region of the boundary layer [11]. The equation governing this principle is given by:

$$Q_{\text{convection}} = hA\Delta T \tag{4}$$

where $Q_{convection}$ is the heat transferred to the flow per unit time through convection, h is the convective heat transfer coefficient, A is the surface area of the sensing element, and ΔT is the temperature difference between the sensing element and the ambient environment.

Also, under ohmic heating, the input power is related to the driving current and the sensor resistance. Since part of the input power is transferred to the flow while the rest is lost conductively through the substrate, the power balance is expressed as

$$I^2R = Q_{\text{conduction}} + Q_{\text{convection}} \tag{5}$$

$$Q_{\text{conduction}} = kA \triangle T \tag{6}$$

where k is the thermal conductivity, I is the driving current and R is resistance of sensing element.

From equation (2), (4), (5) and (6):

$$\triangle T = \frac{I^2R_o}{(k+h)A - \alpha R_o I^2} \tag{7}$$

where I, k, and A remains constant as flow shear stress increases (velocity increases), h is proportional to the square root of the flow velocity, v. Overall, ΔT is approximately proportional to $v^{-1/2}$ due to the cooling effect of the flow at higher flow velocity. This phenomenon leads to a reduction of slew rate seen in output voltage change and shear stress curve, since the output voltage change is proportional to the temperature variation of the resistive sensor.

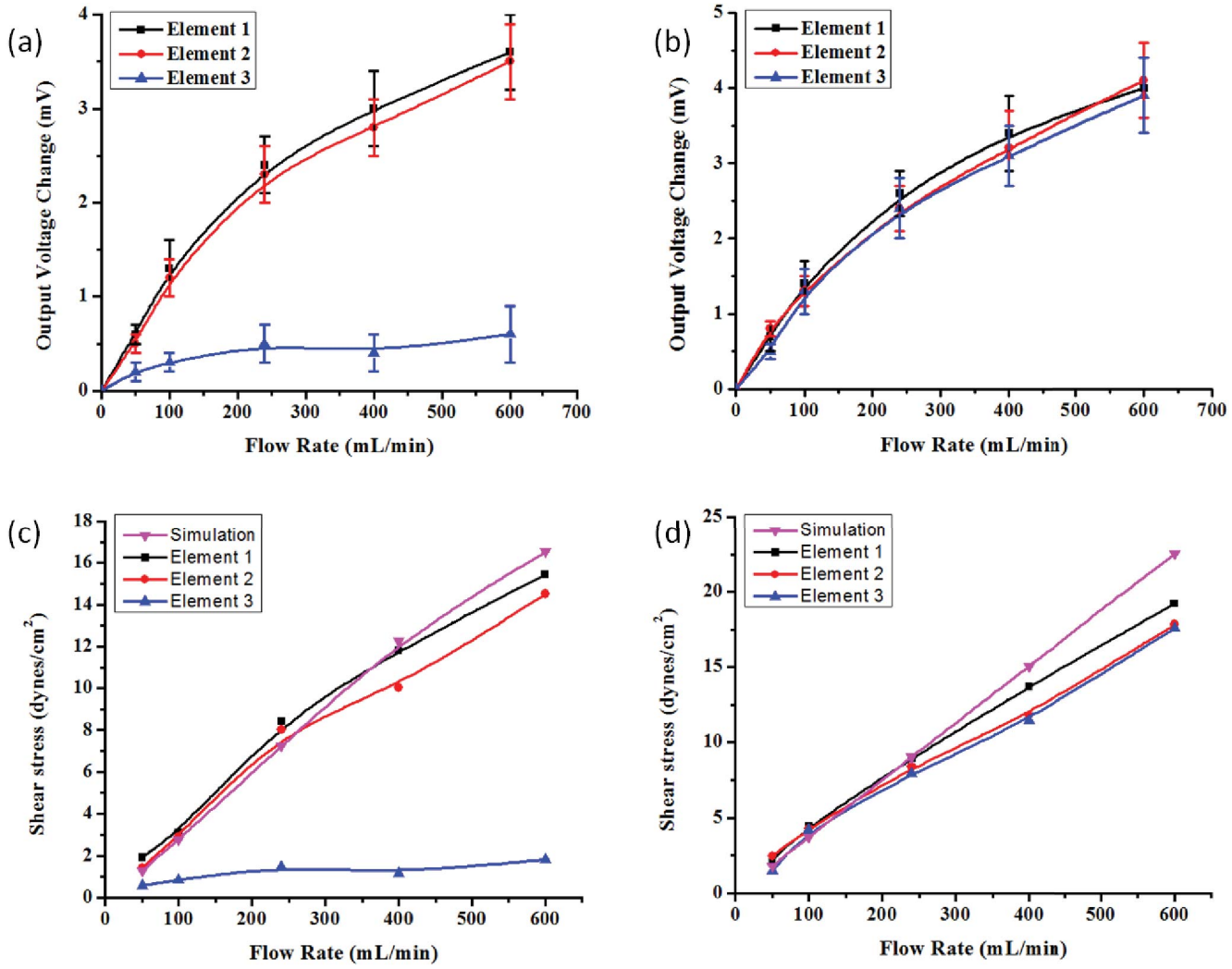

Fig. 9. Experimental results: (a) when 3-D sensor was attached to the wall of flow channel, output voltage for sensing element against the wall changed less than 0.6 mV. The other two sensing elements had maximum 3.3–3.5 mV output voltage change. (b) when 3-D sensor was placed along the center line of the flow channel, output voltage change for all three sensing elements was similar with maximum changes from 3.6 mV to 4 mV. The output voltage change was converted to shear stress with comparison to CFD simulation results, shown in (c) and (d).

On the other hand, similar slew rate reduction of the calibration curve at high flow rate with respect to the relationship between output voltage and wall shear stress was also indicated in reference [8]–[9] for constant-temperature (CT) circuit.

$$\tau_w^{1/3} \propto \frac{V_o^2}{R} \tag{8}$$

where τ_w is the wall shear stress, V_o is the changes in voltage to the thermal sensors as flow past the resistively heated sensor. As previously investigated in reference [6], for both CC and CT circuits, linear relationship between $(V_o^2)/R$ and $\tau_w^{1/3}$ was observed. According to these references, V_o is proportional to $\tau_w^{1/6}$ which agrees with the trend of our calibration curve.

The relationship between the output voltage change and the flow rate were explored, shown in Fig. 9 (a) and (b). When the sensor was placed against the wall of the pipe, the output voltage of element 3 (facing the wall of pipe channel) changed less than 0.6 mV as the flow rate was increased. Meanwhile, the other two sensing elements which were facing the flow field had a maximum output change of 3.3–3.5 mV. On the other hand, when sensor was positioned approximately along the center line of the pipe, all three sensing elements were facing the flow field, far away from the pipe's inner wall. The output voltage changes for all elements were similar with maximum changes from 3.6 mV to 4 mV.

Next, data conversion from the output voltage change to shear stress was realized by using the calibration curve. The experimental results were compared with CFD simulation results, shown in Fig. 9 (c) and (d). With the insertion of the sensor, the wall shear stress will be different from that without the sensor. In previous work [10], the position of catheter and orientation of the sensors have been investigated. Varying the sensor placement from center position to the vessel wall, the shear stress on the sensor wall changed about less than 20%. Our experiment and simulation were implemented in two positions: in the center line and on the wall. Both positions showed the relatively similar response which agreed with the reference. However, the shear stress we obtained from simulation and experiment are sensor-induced stress which is

TABLE I
COMPARISON OF SIMULATION RESULTS BEFORE AND AFTER SENSOR INSERTION

Flow Rate (mL/min)	Wall Shear Stress (No Sensor Insertion) (Dynes/cm^2)	Wall Shear Stress (Sensor in the Center Line) (Dynes/cm^2)
50	0.71	1.81
100	1.47	3.71
240	3.58	9.04
400	5.96	15.06
600	8.95	22.55

different from wall shear stress in the absence of sensor [9]. In order to compensate this variation, simulation results of the flow field before and after the introduction of the sensor in the pipe was calculated at different flow rates, shown in Table 1. A constant ratio of before/after the introduction of the sensor was approximately 2.53 from 50 mL/min to 600 mL/min.

In addition, when comparing all element readings, we can easily notice the difference between elements placed facing the flow field and elements placed against the wall. From the Fig. 9, the element with the largest output signal reading has a relatively accurate result, fitting the CFD simulation better than others especially in the lower shear stress region. All sensing elements show an increasing variation in higher shear stress region due to the cooling effect of the increasing flow velocity. This effect of the decrease in temperature of the resistive element at higher flow velocities can be overcome by incorporating a constant-temperature circuit in lieu of a constant-current circuit.

V. CONCLUSION

In this paper, we developed a novel design and assembly technology for a three-dimensional (3-D) thermal flow sensor to reduce detection error caused by the variation in sensor position within the flow. This sensor is ideally suited to monitor flow properties in narrow and curved geometries, such as a coronary artery, owing to its flexibility, biocompatibility and small size. The unique "fan-shape" sensor design simplifies fabrication and packaging process and ensures the precision of integrating three sensing elements with the catheter. The final product of the 3-D sensor has three independent sensing elements equally distributed around the wall of catheter with 120° spacing. This structure introduces three independent information channels, and cross-comparisons among all readings were utilized to eliminate experimental error and provide better measurement results. The resistance of the sensing elements was measured and the calibration of the sensor was realized in a special designed 2-D PDMS channel and connected with a constant-current circuit. Flow testing was implemented in a pipe at two positions: on the wall or along the center line. When the sensor was in contact with pipe wall, the output voltage of the sensing element facing the pipe wall changed much less than other two sensing elements which were facing the flow field had. Placing the sensors at the center line of the pipe resulted in an almost equal output voltage change for all sensing elements. Computational fluid dynamic (CFD) simulation based on Newtonian fluid properties showed comparable results within an acceptable range of experimental to simulation errors. Therefore, we demonstrated the capability of 3-D thermal flow sensor for detecting the location of the catheter within the channel, by comparing all sensing element readings. And by taking the largest reading, the sensor provides a relative accurate flow measurement in lower flow rate region. In the higher flow rate region (higher flow velocity), the sensitivity was gradually decreased due to the cooling effect of the flow. One possible solution is to replace the constant current readout circuit with a constant temperature circuit which has a negative feedback loop to compensate for the cooling effect at higher flow velocities and maintain the temperature difference of sensing element over ambient temperature.

REFERENCES

[1] L. Rouhanizadeh, D. A. Lin, and T. Hsiai, "Spatial variations in Shear stress at low Reynolds number flow," *Annu. Biomed. Eng.*, vol. 33, no. 10, pp. 1425–1440, 2005.

[2] A. Malek, S. Alper, and S. Izumo, "Hemodynamic shear stress and its role in atherosclerosis," *J. Amer. Med. Assoc.*, vol. 282, pp. 2087–2088, Dec. 1999.

[3] E. Cecchi, C. Giglioli, S. Valente, C. Lazzeri, G. Gensini, R. Abbate, and L. Mannini, "Role of hemodynamic shear stress in cardiovascular disease," *Atherosclerosis*, vol. 214, no. 2, pp. 249–256, Feb. 2011

[4] Q. Lin, F. K. Jiang, X. Q. Wang, Y. Xu, Z. G. Han, Y. C. Tai, J. Lew, and C. M. Ho, "Experiments and simulations of MEMS thermal sensors for wall shear-stress measurements in aerodynamic control applications, " *J. Micromech. Microeng.*, vol. 14, no. 12, pp. 1640–1649, Dec. 2004.

[5] C. Liu, Y. C. Tai, J. B. Huang, and C. M. Ho, "Surface micromachined thermal shear stress sensor," in *Proc. 1st ASME Symp. Appl. Micro-Fabric*, 2006, pp. 1–7.

[6] C. Liu, J. B. Huang, Z. Zhu, F. Jiang, S. Tung, Y. C. Tai, and C. M. Ho, "A micromachined flow shear-stress sensor based on thermal transfer principles," *J. Microelectromech. Syst.*, vol. 8, no. 1, pp. 90–99, Mar. 1999.

[7] Y. Xu, Y. C. Tai, A. Huang, and C. M. Ho, "IC-integrated flexible shearstress sensor skin," *J. Microelectromech. Syst.*, vol. 12, no. 5, pp. 740–747, Oct. 2003.

[8] L. Ai, L. Zhang, W. Dai, C. Hu, K. K. Shung, and T. K. Hsiai, "Real-time assessment of flow reversal in an eccentric arterial stenotic model," *J. Biomech.*, vol. 43, no. 14, pp. 2678–2683, Oct. 2010

[9] N. J. Jen, F. Yu, J. Lee, S. Wasmund, X. Dai, C. Chen, P. Chawareeyawong, Y. M. Yong, R. Li, M. H. Hamdan, and T. K. Hsiai, " Atrial fibrillation pacing decreases intravascular shear stress in a New Zealand white rabbit model: Implications in endothelial function," in *Proc. Biomech. Model Mechanobiol.*, Sep. 2012, pp. 1–3.

[10] L. Ai, H. Yu, W. Takabe, A. Paraboschi, F. Yu, E. S. Kim, R. Li, and T. K. Hsiai, "Optimization of intravascular shear stress assessment in vivo," *J. Biomech.*, vol. 42, no. 10, pp. 1429–1437, Jul. 2009.

[11] E. Meng and Y. C. Tai, "A parylene MEMS flow sensing array," in *Proc. 12th Int. Conf. Solid State Sens., Actuators Microsyst.*, 2003, pp. 686–689.

[12] H. Yu, L. Ai, M. Rouhanizadeh, D. Patel, E. S. Kim, and T. K. Hsiai, "Flexible polymer sensors for in vivo intravascular shear stress analysis," *IEEE/ASME J. Microelectromech. Syst.*, vol. 17, no. 5, pp. 1178–1186, Oct. 2008.

[13] M. A. Schmidt, R. T. Howe, S. D. Senturia, and J. H. Haritonidis, "Design and calibration of a microfabricated floating-element shear-stress sensor," *IEEE Trans. Electron Devices*, vol. 35, no. 6, pp. 750–757, Jun. 1988.

[14] G. Truskey, F. Yuan, and D. Katz, *Transport Phenomena in Biological Systems*. Upper Saddle River, NJ, USA: Pearson Prentice Hall, 2004.

[15] J. H. Haritonnidis, *The Measurement of Shear Stress in Fluid Mechanics Measurement*. New York, NY, USA: Springer-Verlag, 1989, pp. 229–236.
[16] T. Kim, T. Seo, and A. I. Barakat, "Numerical simulations of fluid mechanical interactions between two abdominal aortic branches," *Korea-Austral. Rheol. J.*, vol. 16, no. 2, pp. 75–83, 2004.
[17] B. Mimoun, V. Henneken, P. M. Sarro, and R. Dekker, "Ultra-flexible devices for 360 μm diameter guidewires," in *Proc. IEEE 25th Int. Conf. Micro Electro Mech. Syst.*, Jan. 2011, pp. 472–475.
[18] B. Mimoun, D. van der Voort, A. van der Horst, M. Rutten, F. van de Vosse, and R. Dekker, "Thermal flow sensors on flexible substrates for minimally invasive medical instruments," in *Proc. IEEE Sensors*, Oct. 2012, pp. 1–4.
[19] P. A. L. Tonino, P. H. J. Nico, F. F. William, U. Siebert, F. Ikeno, B. Bornschein, M. van't Veer, V. Klauss, G. Manoharan, T. Engstrøm, K. G. Oldroyd, P. N. Ver Lee, P. A. MacCarthy, and B. De Bruyne, "Fractional flow reserve versus angiography for guiding percutaneous coronary intervention," *N. Engl. J. Med.*, vol. 360, no. 3, pp. 213–224, Jan. 2009

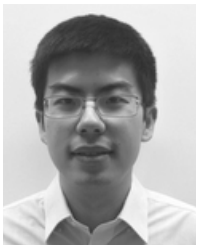

Rui Tang received the B.S. degree from the Huazhong University of Science and Technology, Wuhan, China, in 2009, and the M.S. degree from Arizona State University, Tempe, AZ, USA, in 2011, where he is currently pursuing the Ph.D. degree with the School of Electrical, Computer and Energy Engineering. His current research interests include the development of microelectromechanical systems (MEMS) flow sensors, 3-D MEMS packaging and flexible, stretchable, and foldable skins with integrated sensors and electronics.

Hai Huang received the B.S. and M.S. degrees in electrical engineering from Tsinghua University, Beijing, China, in 2004 and 2007, respectively, and the M.S. degree in electrical engineering from the University of Wisconsin-Madison, Madison, WI, USA, in 2010. He is currently pursuing the Ph.D. degree with the School of Electrical, Computer and Energy Engineering, Arizona State University, Tempe, AZ, USA. His current research interests include miniaturized seismometers for Earth and Moon exploration, microelectromechanical systems (MEMS) accelerometer, flexible, stretchable, foldable electronics and integrated sensors, and 3-D MEMS-NEMS manufacturing and packaging.

Yong Mo Yang received the B.S., M.S., and Ph.D. degrees in electrical engineering from Arizona State University, Tempe, AZ, USA, in 2004, 2007, and 2010, respectively. He is currently with Intel Corporation, San Jose, CA, USA.

Jonathon Oiler received the Ph.D. degree in exploration systems design from the School of Earth and Space Exploration, Arizona State University, Tempe, AZ, USA, in 2013. His current research interests include microelectromechanical systems sensors and electronic systems used for operation in harsh environments. He is currently with Space and Naval Warfare Systems Center, Charleston, SC, USA.

Mengbing Liang received the B.S. degree in electronics science and technology from Huazhong University, Wuhan, China, in 2012. He is currently pursuing the Ph.D. degree with the Department of Electrical Engineering, Arizona State University, Tempe, AZ, USA. His current research interests include metabolic expenditure based accelerometer.

Hongyu Yu received the B.S. and M.S. degrees from Tsinghua University, Beijing, China, in 1997 and 2000, respectively, and the Ph.D. degree from the University of Southern California, Los Angeles, CA, USA, in 2005. He holds the joint position between the School of Earth and Space Exploration and School of Electrical, Computer and Energy Engineering, Arizona State University, Tempe, AZ, USA. His current research interests include microelectromechanical systems for Earth and Space applications with interest on micro seismometer, harsh environment sensing, wireless sensing systems, flexible and stretchable electronics, and manufacture.